PAPER REF: 4678

FLUTTER ANALYSIS OF A COMPOSITE VARIABLE-SPAN WING

Pedro V. Gamboa[1(*)], Pedro D.R. Santos[1], José M.A. Silva[1], Pedro M.B. Santos[1]
[1]LAETA-UBI/AEROG, University of Beira Interior, Covilhã, Portugal
[(*)]*Email:* pgamboa@ubi.pt

ABSTRACT

This paper addresses the aeroelastic study of a composite variable-span morphing wing intended for a small UAV. The study concentrates on the flutter critical speed estimation because of the effects arising due to the interface between fixed and moving wing parts. In this work, modal analysis is performed with ANSYS Structural APDL for obtaining mode shapes and natural frequencies. The critical flutter speed is computed using the typical section in aeroelasticity with unsteady linearized potential theory together with the three-dimensional lifting surface strip theory approximation for lifting surfaces with high aspect ratio. The results show that the wing can fly safely within the intended speed envelope because the critical flutter condition is well above the maximum flight speed.

Keywords: composite materials, structural design, variable-span wing, aeroelasticiy, flutter.

INTRODUCTION

Aircraft morphing concepts have been around since the beginning of aviation, because early flight vehicles were designed based on observations of bird flight. These early concepts were developed and applied primarily for control purposes, but soon it was realized that drastic changes in size and geometry could favor an expanded flight envelope by enabling a single aircraft to perform different missions or to fly in significantly different flight regimes in the same mission (Joshi, 2004). However, most concepts devised and proposed for manned aircraft are heavy and difficult to actuate. With the use of composite materials and new types of actuators it is now possible to develop new concepts which may see practical application in limited shape/size change situations. On the other hand, a new type of vehicle, the Unmanned Air Vehicle (UAV), which has seen a tremendous increase in numbers and applications, both military and civil, is a suitable candidate to receive morphing capabilities that produce more extensive changes in shape and in size.

Aeroelastic instabilities are within the factors that most restrict the flight envelope of aircraft. The simultaneous presence of aerodynamic, inertia, and elastic forces makes it a truly interdisciplinary problem that has been studied since the early days of aviation. The most dangerous aeroelastic phenomenon is flutter, when aerodynamic lifting surfaces suffer a self-excited oscillation that may often be destructive, since the structure absorbs energy from the flow and leads to large amplitude oscillations of the lifting body. Due to its catastrophic nature, it is imperative that the occurrence of flutter on lifting surfaces is avoided to prevent failure of the structure due to large deformation from occurring. The mission profile of the next generation of UAVs will lead to a design requirement of an adaptable airframe to best meet the varying flight conditions. It is conceivable that the changes in geometry would also incur in aeroelastic instabilities, such as flutter, at points of transition during the mission (Rubillo, 2006). On the other hand, the reduction of structural stiffness that may be required to allow the geometric changes is also an important factor in producing instabilities at lower

flight speeds. Various morphing wing concepts have been studied, analyzed and tested for aeroelastic performance design and evaluation (Bae, 2004; Snyder, 2005; Lee, 2005; Andersen, 2007).

This paper addresses the aeroelastic analysis of a composite variable-span morphing wing (VSW) for a small UAV which provides improved flight efficiency in an extended operational speed range, relative to a conventional fixed wing, by symmetrically adjusting the wing span to the flight speed. The analysis work is divided into two main parts: (1) calculation of mode shapes and frequencies of natural vibration; (2) computation of flutter critical speed and considerations about the aeroelastic behavior of the wing in particular the effects arising due to interfaces between fixed and moving wing parts.

AEROELASTIC MODEL

The flutter study uses complex determinant analysis to determine the combination of airspeed and frequency for which the neutrally damped motion is sustained. The computational analysis of this phenomenon requires the following steps: (a) building the structural model and performing a modal analysis; (b) generating strip section data (inertia, elastic); (c) computing aerodynamic coefficients; and, finally, (d) solving the flutter determinant. An explanation on the first and second steps is given later. The third and fourth steps are briefly described in the following paragraphs.

The typical section using unsteady linearized potential theory together with the strip theory aerodynamic simplification is used to estimate the aeroelastic characteristics of a straight, high aspect ratio wing.

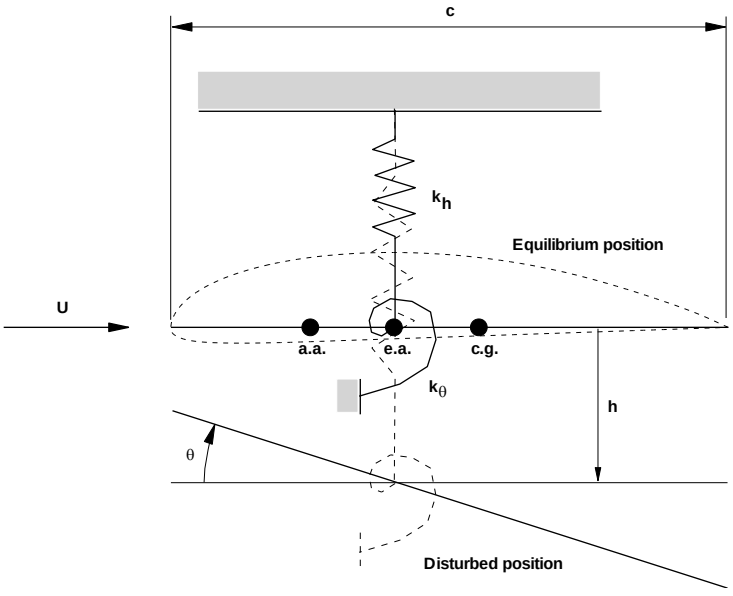

Fig.1 Typical section of the aeroelastic lifting surface

The determination of the aerodynamic forces acting on an airfoil moving in an unsteady motion about its initial state of equilibrium is complex. At any instant in time, the change in the airfoil position results in a change in the circulation around the airfoil which causes a change in the vortex shed from its trailing edge. This vortex shedding produces vertical

velocities on the airfoil and affects the incremental non-stationary aerodynamic loads on the lifting section. At the critical point of dynamic instability, the motion of such a system is a pure harmonic oscillation. From this fact, a formulation to compute the incremental non-stationary aerodynamic loads has been established which presents the exact solution at the critical instability condition. The linearized incremental lift and moment acting on a two-dimensional airfoil performing a simple harmonic motion in two degrees of freedom (airfoil vertical displacement and airfoil rotation) has been obtained by other authors (Theodorsen, 1934; Theodorsen, 1940). In Fig. 1 the typical section is shown with the main parameters necessary to characterize its dynamic motion.

The typical section theory is extended for the computation of the aeroelastic stability of a three-dimensional lifting surface at low speeds with no considerable mass concentration areas using the strip theory aerodynamic simplification (Scanlan, 1948). The strip theory approximation for lifting surfaces of high aspect ratio consists in dividing the lifting surface in chordwise small strips of finite width and assuming that at each strip the flow is two-dimensional and does not interact with the flow of other strips.

Consider a lifting surface divided into strips of width Δy_i, mean chord c_i and lateral position y_i. For each strip of the wing the mass per unit width, m, the moment of inertia about the elastic axis (e.a.) per unit width, i_θ, the static mass moment about the e.a. per unit width, s_θ, the bending stiffness, EI, and the torsional stiffness, GJ, are known quantities.

The Lagrange equations of motion of the complete wing are

$$\begin{aligned} M\ddot{h} + S_\theta\ddot{\theta} + C_h\dot{h} + K_h h &= Q_h \\ I_\theta\ddot{\theta} + S_\theta\ddot{h} + C_\theta\dot{\theta} + K_\theta\theta &= Q_\theta \end{aligned} \tag{1}$$

where M is the total mass of the wing, S_θ is the total static mass about the elastic axis, I_θ is the total moment of inertia about the e.a., K_h is the total stiffness in bending and K_θ is the total stiffness in rotation. These quantities can be computed from

$$\begin{aligned} M &= \int_0^l m(y)[f_h(y)]^2\,dy \\ S_\theta &= \int_0^l s_\theta(y)\,f_h(y)\,f_\theta(y)dy \\ I_\theta &= \int_0^l i_\theta(y)[f_\theta(y)]^2\,dy \\ K_h &= \int_0^l EI(y)\left[\frac{\partial^2}{\partial y^2}f_h(y)\right]^2 dy \\ K_\theta &= \int_0^l GJ(y)\left[\frac{\partial^2}{\partial y^2}f_\theta(y)\right]^2 dy \end{aligned} \tag{2}$$

where $f_h(y)$ and $f_\theta(y)$ are the assumed shapes of the first uncoupled bending and torsion modes of vibration, respectively, normalized to unit values at the wing tip.

In Eq. (1), C_h and C_θ are the viscous damping coefficients, which are assumed zero in this work, and Q_h and Q_θ are the generalized incremental aerodynamic loads given by

$$\begin{Bmatrix} Q_h \\ Q_\theta \end{Bmatrix} = \pi\rho\omega^2 \begin{bmatrix} A_{hh} & A_{h\theta} \\ A_{\theta h} & A_{\theta\theta} \end{bmatrix} \begin{Bmatrix} \underline{h} \\ \underline{\theta} \end{Bmatrix} \tag{3}$$

where ω is the coupled frequency of vibration of the system and the elements A_{hh}, $M_{h\theta}$, $L_{\theta h}$ and $M_{\theta\theta}$ are functions of the wing chord and wing span sizes, the elastic axis position, the normalized bending and torsion mode shapes and the complex unsteady aerodynamic coefficients (Scanlan, 1948) that are functions of the reduced frequency

$$k = \frac{\omega c}{2U} \tag{4}$$

where c is taken as the wing chord at 2/3 of the semi-span and U is de flow velocity. The integrals of Eq. (2) are calculated from the root to the tip, where the semi-span is represented by l, by applying a sum through all the strips considered.

Because the oscillation is harmonic at the critical condition, the solution of the equations of motion can be written in the form

$$\underline{h} = h_0 e^{i\omega t} \quad ; \quad \underline{\theta} = \theta_0 e^{i\omega t} \tag{5}$$

which on substitution into Eqs. (1) leads to the final system of equations representing the vibration of the wing as

$$\begin{bmatrix} \overline{A}_{hh} - \Omega_h Z & \overline{A}_{h\theta} \\ \overline{A}_{\theta h} & \overline{A}_{\theta\theta} - Z \end{bmatrix} \begin{Bmatrix} h_0 \\ \theta_0 \end{Bmatrix} = \begin{Bmatrix} 0 \\ 0 \end{Bmatrix} \tag{6}$$

where $\overline{A}_{h\theta}$, $\overline{A}_{h\theta}$, $\overline{A}_{\theta h}$ and $\overline{A}_{\theta\theta}$ are functions of M, S_θ, I_θ, the air density and the A elements of Eq. (3) (Scalan, 1948) and

$$\begin{gathered} Z = X - iY \quad \text{with} \quad X = \left(\frac{\omega_\theta}{\omega}\right)^2 \quad ; \quad Y = gX \\ \Omega_h = \left(\frac{\omega_h}{\omega_\theta}\right)^2 \end{gathered} \tag{7}$$

where ω_h and ω_θ are the uncoupled natural frequencies in bending and in torsion, respectively, and g is the damping coefficient.

For the nontrivial solution of Eq. (6), its determinant must be zero, thus

$$\Delta = \begin{vmatrix} \overline{A}_{hh} - \Omega_h Z & \overline{A}_{h\theta} \\ \overline{A}_{\theta h} & \overline{A}_{\theta\theta} - Z \end{vmatrix} = 0 \tag{8}$$

The flutter boundary is provided when the value of damping is equal to zero. A technique of reduced frequency sweeps is used. The sweeping starts from zero reduced frequency of the unsteady aerodynamic forces with an increment up to a maximum selected value. Eq. (8) is solved for Z and its real and imaginary parts, X and Y, respectively, are extracted. The frequency, damping and speed are then obtained from Eqs. (7) and (4) in the form

$$\omega = \frac{\omega_\theta}{\sqrt{X}} \quad ; \quad g = \frac{Y}{Z} \quad ; \quad U = \frac{\omega c}{2k} \tag{9}$$

Then, the curves of U-g and U-ω can be plotted.

The determinant of Eq. (8) is a second order polynomial in Z. Therefore, two values of ω and g are obtained for each k selected, being the flutter curve the one for which g becomes zero at a lower value of $1/k$. At this point, where the system is neutrally damped, the critical flutter condition is obtained as

$$\omega_f = \frac{\omega_\theta}{\sqrt{X}} \quad ; \quad U_f = \frac{\omega_f c}{2k} \tag{10}$$

The uncoupled natural frequencies of vibration can be either calculated from the results of Eq. (2) with

$$\omega_a = \sqrt{\frac{K_h}{M}} \quad ; \quad \omega_\theta = \sqrt{\frac{K_\theta}{I_\theta}} \tag{11}$$

or from a modal analysis.

THE VARIABLE SPAN WING

The shape and size of the variable-span morphing wing (VSW) was obtained through a computational constrained aerodynamic shape optimization aimed at determining the wing chord and span values that minimized its drag for a given speed range. The geometric constraints imposed on the wing design optimization were dictated by component fitting, manufacturing simplicity and mechanism functionality considerations. A detailed description of the aerodynamic optimization procedure and results is given in (Mestrinho, 2011). The actuation mechanism, wing structure and manufacturing techniques used to build the structure of the wing prototype are presented in (Felício, 2011).

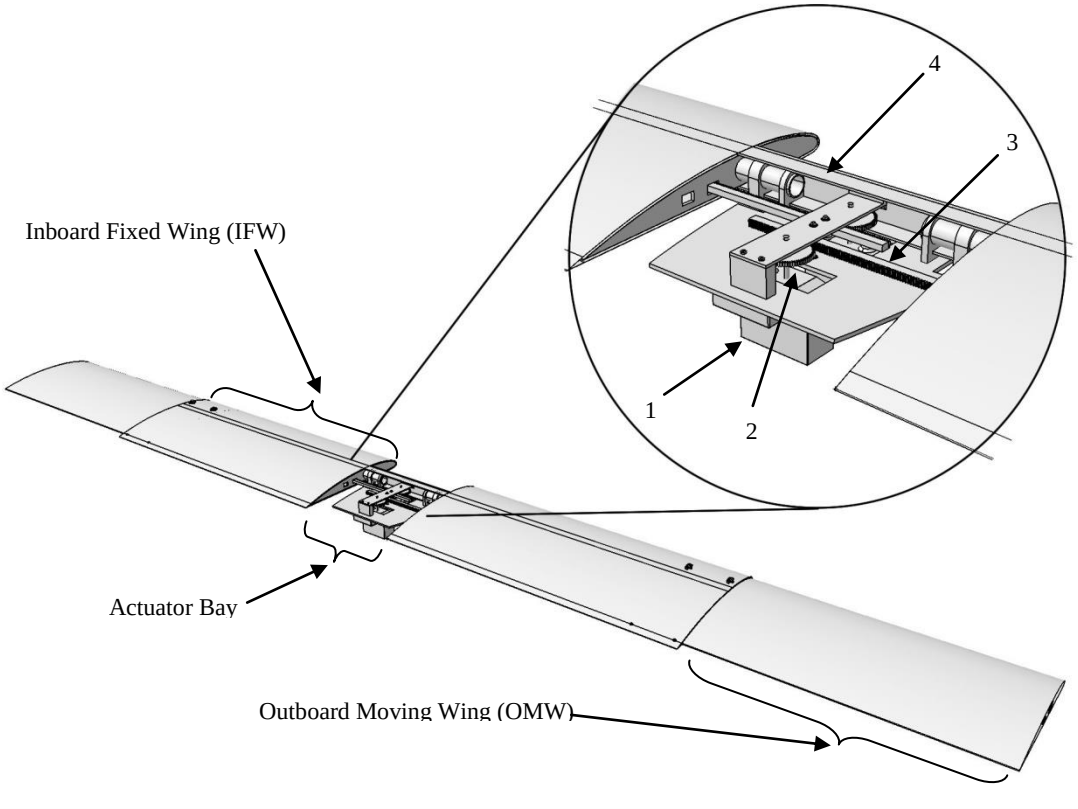

Fig.2 General CAD view of the Variable-Span Wing (VSW) showing its main components and a detail of the actuator bay: (1) servo-motor; (2) transmission pinion; (3) transmission rack; and (4) pultruded unidirectional carbon spar

Wing Concept

The variable-span wing concept in the present work exhibits a very simple layout: a hollow wing, the inboard fixed wing (IFW), inside of which a smaller conventional wing, outboard moving wing (OMW), slides actuated by a simple electromechanical mechanism consisting of a servomotor, a pinion and rack. The minimum span is about 1.5m and the maximum span is 2.5m. When fully extended, both inboard and outboard wing parts have a length of 0.625m and a 0.1m of minimum wing overlapping provides sufficient wing stiffness in the full extended configuration. The overall system was developed in a CAD/CAM tool (Felício, 2011) and is illustrated in Fig. 2 where the main components are highlighted.

Both wing parts are of constant chord length which facilitates manufacture and makes the fitting and support of the outboard wing easier to implement. The chord length of the IFW is larger to allow the OMW to fit inside it. Their values are 0.266m and 0.245m, for the IFW and the OMW, respectively.

Materials and Structural Concept

The structural components of the wing were developed with a combination of composite materials and hard and soft wood which provide good general strength and stiffness.

The IFW uses a monocoque type of structure with a sandwich skin of carbon/foam/carbon which is required to both provide the correct shape and resist shear loads. From inside out, the load carrying thick skin has a layer of 48g/m^2 glass/epoxy, a layer of 185g/m^2 carbon/epoxy, a layer of 2mm porous PVC foam (55kg/m^3), a layer of 185g/m^2 carbon/epoxy, and finally another layer of 48g/m^2 glass/epoxy. The PVC foam core was incorporated between the carbon fibre layers to allow embedding of the main spar and to give adequate stiffness to the skin. All fibre fabric layers are plain weave oriented at 0deg along the wing span. The glass layers do not have a structural role but are added to reduce the porosity of the carbon/epoxy layers. The complete assembled skin has a thickness of 2.5mm, which creates a fairly acceptable small discontinuity between the IFW and the OMW. Spar caps inside the IFW are composed of rectangular beams made of pultruded carbon fibre with a cross-section of 16mm $\times$ 1.7mm. For greater strength and stiffness the spar extends along the complete fixed wing a 1.475m span. This can be observed in Fig. 2. The properties of the different materials used in the VSW structure are summarized in Table 1.

The total length of the OMW is 625mm, where 525mm is the stroke and 100mm is the overlap with the remaining IFW so that bending and torsion moments can be effectively transmitted from the OMW to the IFW. The structural configuration used in the moving wing part is very conventional: the wing is composed of ten 2mm thick balsawood ribs, a 240g/m^2 carbon fibre/epoxy skin and a I-section spar consisting of 8mmx0.8mm pultruded carbon spar caps with a 1.5mm balsa wood spar web. The main spar confers sufficient bending stiffness while the ribs provide the correct wing shape. The ribs are bonded to both the skin and spar with epoxy glue.

The cross-sections of the wing are represented in Fig. 3 clearly showing the different structural layouts adopted for the inboard and outboard parts of the wing as necessary to allow the motion of the OMW inside the IFW. The circular tubes in the OMW allow the span actuation system components to move inside it and although they have no special structural function they do increase the stiffness of the OMW particularly in bending.

Table 1 Material properties

Property	Wooven carbon/epoxy	Pultruded carbon/epoxy	Balsa wood	PVC foam (Airex C70.55)
ρ, kg/m^3	1600	1500	120	55
E_1, GPa	51	120	1.28	0.045
E_2, GPa	51	8	0.0192	0.045
G, GPa	5	5	0.04736	0.022
ν_{12}	0.1	0.3	0.488	0.0227
ν_{23}	0.1	0.3	0.231	0.0227

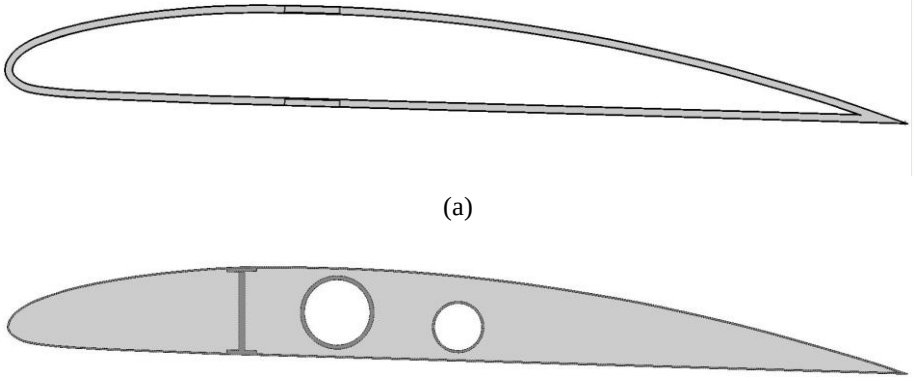

(a)

(b)

Fig.3 Wing cross-sections: (a) IFW and (b) OMW

Numerical Model

The VSW wing is modeled in ANSYS Structural APDL using shell and beam elements according to the model shown in Fig. 3. The finite element model (FEM) of the IFW is discretized using SHELL181 type elements. The sandwich skin is modeled with three layers built as offset surfaces from the airfoil contour according to its own thickness. These three layers constitute the carbon epoxy and PVC sandwich. In the locations of the embedded spar, the PVC foam layer is replaced with unidirectional pultruded carbon-epoxy. Likewise, the OMW skins, ribs, I shape spar web and circular spar are discretized using SHELL181 type elements. The OMW I-section spar cap is discretized using BEAM188 elements.

The SHELL181 element is suitable for analyzing thin to moderately thick shell structures. It is a four-node element with six degrees of freedom at each node: translations in the *x*, *y*, and *z* directions, and rotations about the *x*, *y*, and *z*-axes. This type of element is well-suited for linear, large rotation, and/or large strain nonlinear applications. Additionally, the change in shell thickness is taken into account in nonlinear analyzes. Regarding the BEAM188 element, this is suitable for analyzing slender to moderately stubby/thick beam structures. This is a linear, quadratic, or cubic two-node 3D beam element. BEAM188 has six degrees of freedom at each node. These include translations in the *x*, *y*, and *z* directions and rotations about the *x*, *y*, and *z* directions. This element is well-suited for linear, large rotation, and/or large strain nonlinear applications.

The contact in the overlap surface between the IFW and the OMW is modeled with a shell to

shell contact, using TARGE170 (target element for 3D geometries) and CONTA173 (contact element for 3D shells without mid side nodes). Since the distinction between the contact and target surfaces is not clear in the interface, a symmetric contact (or "two-pass contact") is created. In this type of contact, each surface is designated to be both a target and a contact surface. Then, two sets of contact pairs between the contacting surfaces are generated. The symmetric contact is less efficient than asymmetric contact. Another reason to use this type of contact in this particular situation is to reduce penetration between contact surfaces. Throughout the work two types of behavior of the contact elements are used: standard and bonded (always). The former is used when it is required to simulate the flexible contact on the VSW interface. The latter, as the name infers, is used to simulate a rigid connection in the interface.

The wing is considered to be built-in near the root vicinity. Additionally, the center portion of the inner most rib of the OMW is constrained along the *y*-axis to simulate the constraint imposed by the rack and pinion actuator mechanism and thus prevent the OMW from sliding outwards. The complete assembled finite element model is shown in Fig. 4.

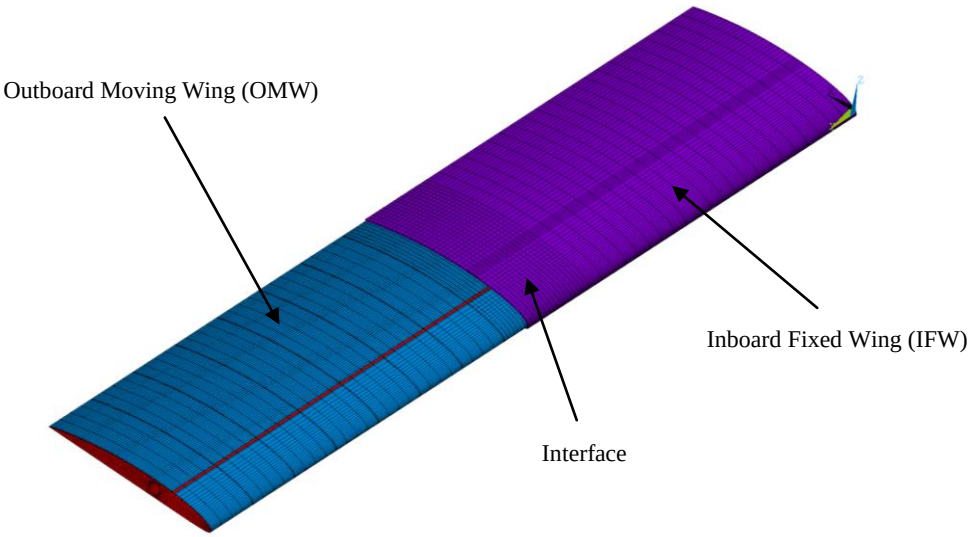

Fig.4 Mesh of the finite element model

A convergence analysis for a free vibration analysis of the finite element resulting model was carried out with several grid mesh sizes. During this study, the contact between the IFW and OMW was considered to be rigidly bonded. The refinement of the grid mesh was done by changing the default element size in ANSYS. Figure 5 shows the convergence of the first six modal frequencies for several mesh sizes. It is possible to conclude that the first four modal frequencies show a stabilized result for a mesh with 31000 elements. Therefore, the results obtained in the following analysis are obtained for mesh grid with this number of elements.

RESULTS AND DISCUSSION

Due to the flexible nature of the interface between the two parts of the wing, two situations are analyzed: one corresponding to the initially built wing prototype and another with an interface assumed to be much stiffer as explained above to represent a stiffener placed around the tip of the IFW section in the shape of a wing fence. The effect of this rigid interface is to

prevent the sandwich skin to bend thus reducing the amount of rotation in bending which the outer wing part experiences.

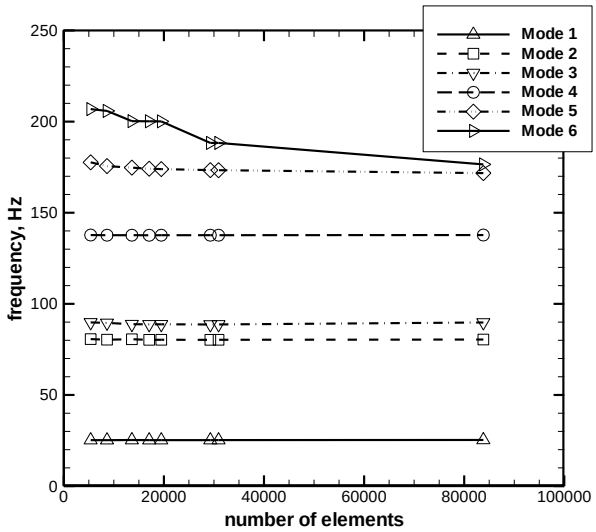

Fig.5 First six modal frequencies obtained using different numberr of elements

Mode Shapes and Natural Frequencies

A linear perturbation modal analysis (ANSYS®, 2011) is performed using at the initial state a static wing deformation induced by the aerodynamic loading in cruise. The first four mode shapes obtained are shown in Fig. 6. Essentially, the mode shapes are similar irrespective of the interface between the IFW and the OMW (flexible or rigidly bonded). The first two modes are practically pure bending modes, particularly in the wing with the rigid interface. The third mode in both types of interface is a pure torsion mode. The fourth mode is a bending mode in the horizontal *x-y* plane. In the second mode, an increase in the bending curvature is observed at the IFW/OMW interface region where the wing is less rigid in bending. The difference in the two types of interface has little effect on the torsion mode because, unlike in the bending case, the torsion motion does not make the upper and lower skins move slightly apart at the interface thus restricting the amplitude of the deflection.

Regarding the natural vibration frequencies the large difference in the two types of interface occurs between the bending modes (mode 1, mode 2 and mode 4). In the first torsion mode (mode 3) there is only a reduction of 3.6% due to the less rigid interface. Table 2 summarizes the frequencies of the first four mode shapes in the two interface cases.

Table 2 First four natural frequencies of vibration in Hz (or rad/s)

Mode	VSW interface	Rigid interface
1	17.93 (112.7)	25.24 (158.6)
2	57.94 (364.1)	80.28 (504.1)
3	85.49 (537.2)	88.72 (557.4)
4	107.33 (674.4)	137.67 (865.0)

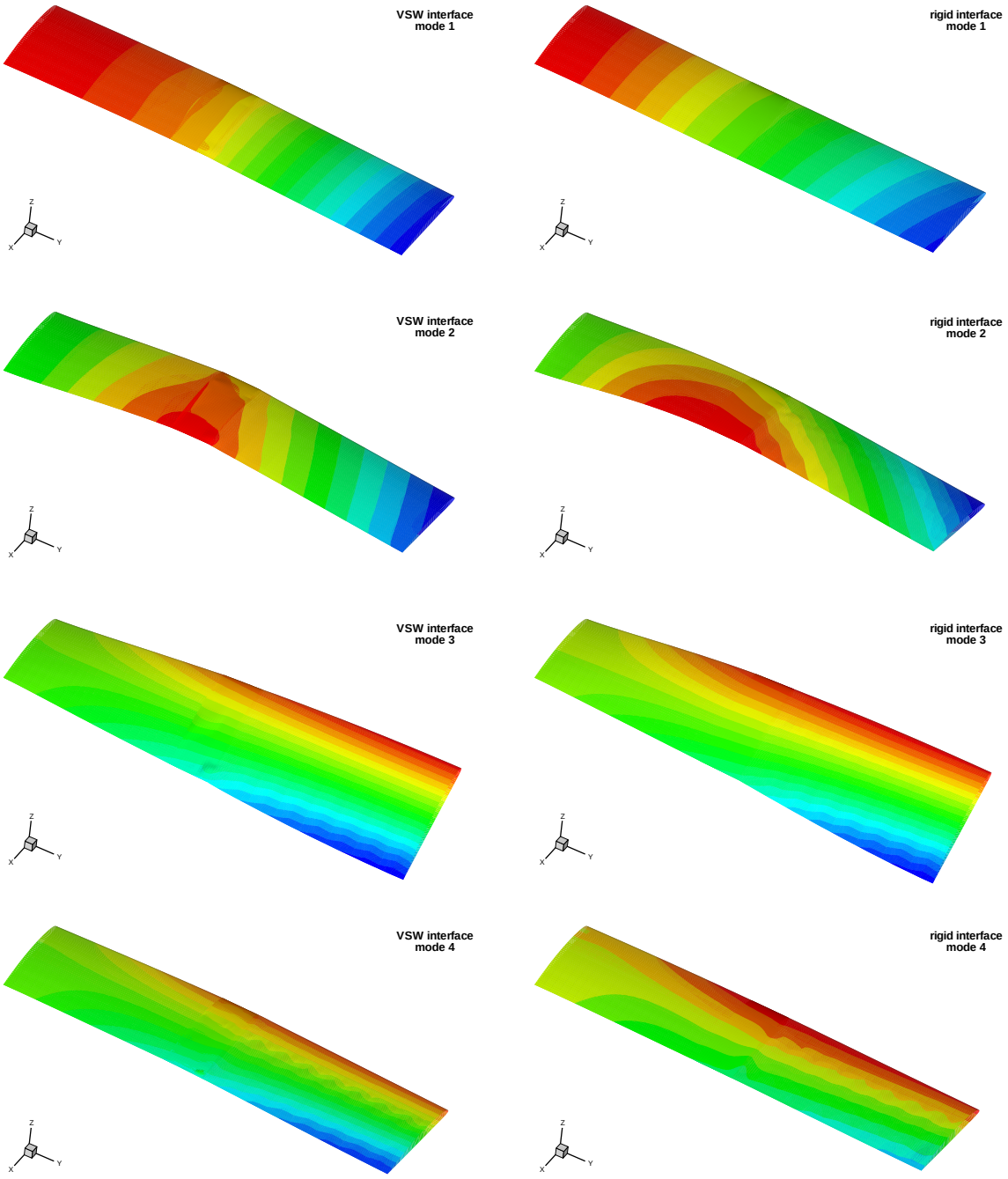

(a) (b)

Fig.6 First four mode shapes of natural vibration of the wing fully extended (a) with elastic VSW interface (19.9Hz, 57.9Hz, 85.5Hz and 107.3Hz) and (b) with rigid interface (25.2Hz, 80.3Hz, 88.7Hz and 137.7Hz)

From the data obtained by the numerical modal analysis, vertical deflections and rotations of and about the elastic axis were extracted to produce 2-dimensional, beam-like, bending and torsion modes. Figure 7 illustrates the first and third mode shapes scaled to unit value at the wing tip. There is a noticeable effect from the different modeling of the interface on the bending mode. The curvature at the VSW interface is increased owing to the reduced stiffness implemented in this region in the numerical model (Santos, 2013). On the other hand, the

torsion behavior is hardly altered, fact that can also be observed from the natural vibration frequencies. These mode shape curves in Fig. 7 are used in the flutter model to estimate the flutter critical speed and frequency for the two types of interface.

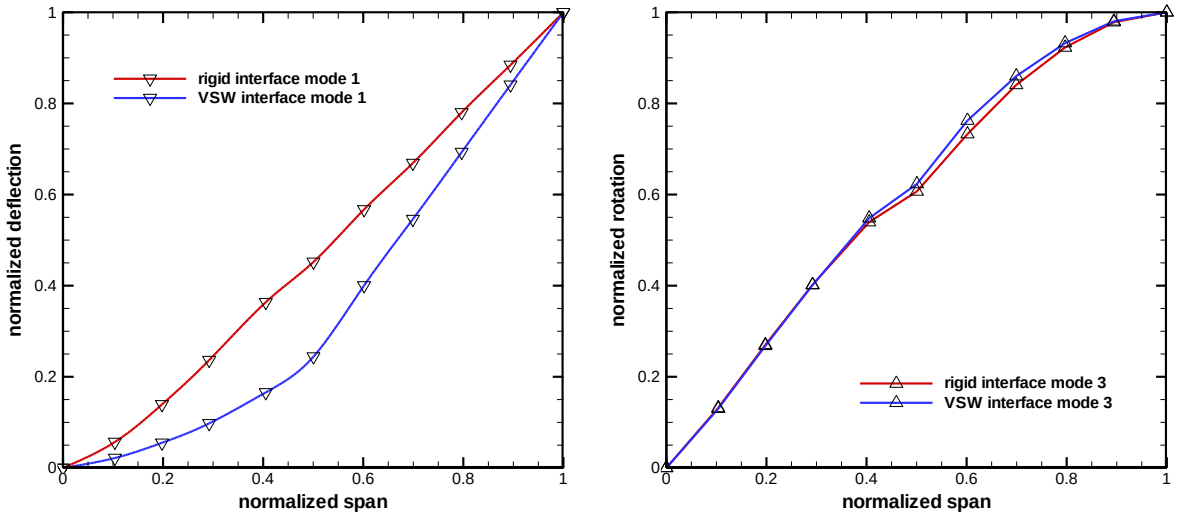

(a) (b)

Fig.7 Mode shapes at the elastic axis for both types of interface: (a) bending $f_h(y)$ and (b) torsion $f_\theta(y)$

Flutter Speed

Flutter analysis is performed for sea level standard conditions where the air density is greatest and the flutter critical speed will be lowest.

Some parameters of the wing section are required to be available in order to perform the flutter analysis. These parameters are shown in Table 3 for the three different sections available in the wing, namely the IFW, the OMW and the interface of the two. The elastic axis position on the chord is estimated from the numerical FEM model by applying a pure couple at the tip of the wing and observing the line along the span that does not suffer any vertical displacement. The mass properties and center of gravity position are obtained through calculations and confirmed experimentally from the wing prototype. Calculation of the static mass moment and mass moment of inertia follow by taking the moment of the mass about the elastic center and by multiplying the mass by the squared distance to the e.a., respectively. A total of ten segments along the span are used to represent the wing's varying characteristics and the local parameter values for each one are interpolated as required. The natural uncoupled frequencies are those obtained from the modal analysis.

Figure 8(a) represents the *U-g* diagram for the wing with different interface rigidity. Positive and negative damping values are representative of unstable and stable conditions, respectively. As we can see, flutter occurs when the velocity curve intersects the zero damping line. This means that at this velocity, if the structure suffers an excitation, the aerodynamic flow will no longer damp the structural vibration. One is then able to determine the flutter frequency of the model using the plot of *U-ω* from Fig. 8(b) and picking off the frequency value of the unstable mode at the flutter velocity value. The slope of the damping versus velocity curve as it passes through flutter velocity can be thought of as a qualitative measure of how violently the oscillations would occur during accelerated flight.

Table 3 Wing section properties

Parameter	IFW section	interface	OMW section
c, m	0.266	0.266	0.245
x_e/c	0.371	0.368	0.365
x_{cg}/c	0.464	0.455	0.445
m, kg/m	0.613	1.030	0.417
s_θ, kg	15.16×10^{-3}	23.61×10^{-3}	8.10×10^{-3}
i_θ, kg.m	0.375×10^{-3}	0.541×10^{-3}	0.158×10^{-3}

The first bending mode (mode 1) and the first torsion mode (mode 3) are used to compute the flutter critical speed since these are the uncoupled natural modes with the lowest frequencies. The critical mode, as seen from Fig. 8(a), is the torsion mode because its damping becomes zero before that of the bending mode. Typically this is the case in aircraft lifting surfaces. As expected, the effect of a less rigid interface between the OMW and the IFW is to reduce the flutter critical speed. Even though not so significant, the reduction in the bending natural frequency results in a decrease of 4.2% in U_f from 60.36m/s for the wing with the rigid interface to 57.81m/s for the VSW interface. The flutter critical frequency of the rigid interface wing is 33.95Hz (213.4rad/s) whist the flutter frequency of the VSW interface is 25.48Hz (160.1rad/s), as observed from Fig. 8(b).

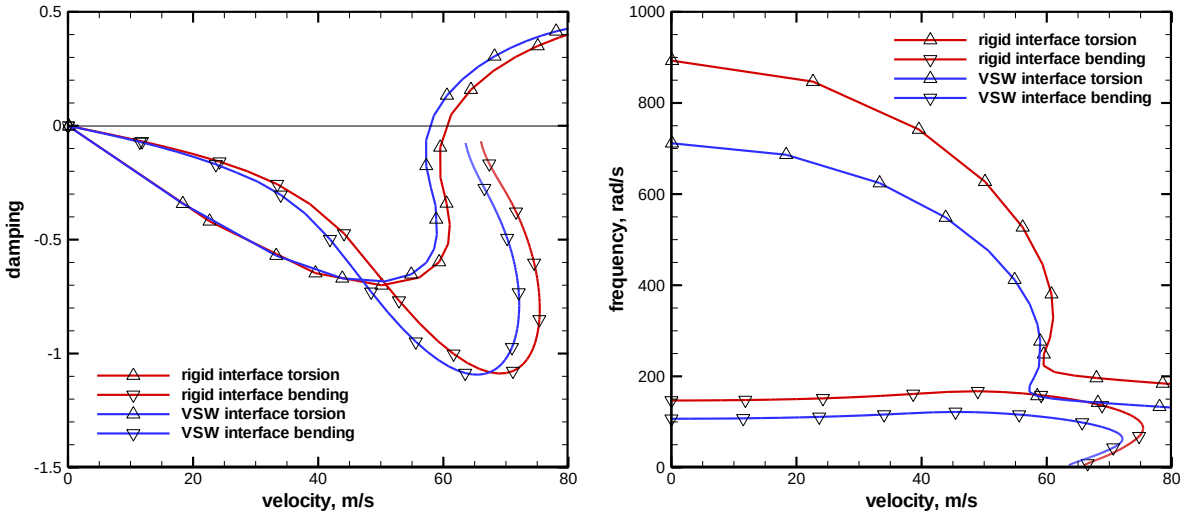

(a) (b)

Fig.8 Damping and frequency results for the two types of wing interface: (a) *U-g* diagram and (b) *U-ω* diagram

The normal cruise speed ranges from 20m/s to 35m/s and the intended maximum speed for the variable-span wing is 40m/s and (Mestrinho, 2011). From the results obtained in this study, a speed margin of 44.5% ensures safe operations of the VSW during the planned flight tests programme.

CONCLUSIONS

A numerical model of a newly developed composite variable-span wing was developed in ANSYS Structural APDL to compute its mode shapes and frequencies of free vibration and a flutter model using the typical section in aeroelasticity with unsteady linearized potential theory. Also, three-dimensional lifting surface strip theory approximation for lifting surfaces was implemented to estimate the critical flutter speed.

The effect of loss of rigidity in the interface between the IFW and the OMW, necessary to perform the required span extensions and retractions, has a negative impact on the critical flutter speed. Nevertheless, the flutter analysis undertaken in this work allowed to conclude that the flight speed envelope required for the UAV under consideration is still viable for the proposed structural design of the VSW concept.

Experimental testing of the wing will be pursued to validate de variable-span wing concept in terms of aeroelastic characteristics and to help establish a scheme for the design and analysis of this new morphing capable type of wing.

ACKNOWLEDGMENTS

The work presented herein has been partially funded by the European Community's Seventh Framework Programme (FP7) under the Grant Agreement 314139. The CHANGE project (Combined morphing assessment software using flight envelope data and mission based morphing prototype wing development) is a Level 1 project funded under the topic AAT.2012.1.1-2. involving 9 partners. The project started on August 1st 2012.

REFERENCES

Andersen GR, Coean DL, Piatak DJ. Aeroelastic Modeling, Analysis and Testing of a Morphing Wing Structure. 48th AIAA/ASME/ASCE/AHS/ASC Structures, Structural Dynamics & Materials Conference. Honolulu, Hawaii, 23-26 April 2007.

ANSYS® Academic Research, Release 14.0, Mechanical APDL Structural Analysis Guide, Chapter 9, ANSYS, Inc. 2011.

Bae J-S, Seigler TM, Inman DJ. Aerodynamic and Aeroelastic Considerations of a Variable-Span Morphing Wing. 45th AIAA/ASME/ASCE/AHS/ASC Structures, Structural Dynamics & Materials Conference. Palm Springs, California, 19-22 April 2004.

Felício J, Santos P, Gamboa P, Silvestre M. Evaluation of a Variable-Span Morphing Wing for a Small UAV. 52th AIAA/ASME/ASCE/AHS/ASC Structures, Structural Dynamics and Materials Conference, Denver, Colorado, 4-7 April, 2011.

Joshi S, Tidwell T, Crossley W, Ramakrishnan S. Comparison of Morphing Wing Strategies Based Upon Aircraft Performance Impacts. 45th AIAA/ASME/ASCE/AHS/ASC Structures, Structural Dynamics and Materials Conference, Palm Springs, California, April 19-22, 2004.

Lee DH, Weisshaar TA. Aeroelastic Studies on a Folding Wing Configuration. 46th AIAA/ASME/ASCE/AHS/ASC Structures, Structural Dynamics & Materials Conference. Austin, Texas, 18-21 April 2005.

Mestrinho J, Gamboa P, Santos P. Design Optimization of a Variable-Span Morphing Wing

for a Small UAV. 52th AIAA/ASME/ASCE/AHS/ASC Structures, Structural Dynamics and Materials Conference, Denver, Colorado, 4-7 April, 2011.

Rubillo C, Marzocca P, Bollt E. Active Aeroelastic Control of Lifting Surfaces via Jet Reaction Limiter Control. International Journal of Bifurcation and Chaos, 2006, 16(9), p. 2559-2574.

Santos PD, Gamboa P, Santos PM, Silva JM. Structural Design of a Composite Variable-Span Wing. 4th International Conference on Integrity, Reliability and Failure, Funchal, 23-27 June 2013.

Scanlan RH, Rosenbaum R. Outline of an Acceptable Method of Vibration and Flutter Analysis for a Conventional Airplane. Airframe and Equipment Engineering Report No. 43 and Aviation Safety Release No. 302, 1948.

Snyder MP, Sanders B, Estep FE, Frank GJ. Vibration and Flutter Characteristics of a Folding Wing. 46th AIAA/ASME/ASCE/AHS/ASC Structures, Structural Dynamics & Materials Conference, Austin, Texas, 18-21 April 2005.

Theodorsen T. General Theory of Aerodynamic Instability and the Mechanism of Flutter. NACA Technical Report No. 496, 1934.

Theodorsen T, Garrick IE. Mechanism of Flutter, A Theoretical and Experimental Investigation of the Flutter Problem. NACA Technical Report No. 685, 1940.